DOI: 10.1002/chem.200701538

Crystal-Packing-Induced Antiferromagnetic Interactions of Metallocenes: Cyanonickelocenes, -cobaltocenes, and -ferrocenes

Sandra Altmannshofer,[a] Eberhardt Herdtweck,[b] Frank H. Köhler,*[b] Robert Miller,[a] Rüdiger Mölle,[b] Ernst-Wilhelm Scheidt,[a] Wolfgang Scherer,[a] and Cyrille Train[c]

Abstract: The cyano-substituted metallocenes $[M(C_5H_4CN)_2]$ (M = Fe, **1**; Co, **2**; Ni **3**) and $[M(C_5Me_5)(C_5H_4CN)]$ (M = Fe, **4**; Co, **5**; Ni, **6**) were synthesized in yields up to 58% by treating $K(C_5H_4CN)$ or $Tl(C_5H_4CN)$ with suitable transition-metal precursors. Cyclic voltammetry indicated that the oxidation and reduction potentials of all the cyanometallocenes were shifted to positive values by up to 0.8 V. Single-crystal X-ray structure analysis showed that **1** had eclipsed ligands, formed planes in the lattice, and—unlike usual metallocenes—lined up in stacks perpendicular to these planes. Powder X-ray studies established that **1** and **2** are isotypic. The ^1H and ^{13}C NMR spectra were recorded for all the new compounds. Signal shifts of up to $\delta =$ 1500 ppm were recorded for the paramagnetic molecules **2** and **3** and were, at a given temperature, strikingly different for solution and solid-state spectra. These results pointed to antiferromagnetic interactions as a consequence of molecular ordering in the lattice, as confirmed by magnetic measurements. The temperature-dependent susceptibilities were reproduced by Heisenberg spin-chain models ($H = -J \sum_{i=1}^{n-1} S_i S_{i+1}$), thus yielding $J = -28.3$ and $-10.3\ cm^{-1}$ for **2** and **3**, respectively, whereas $J = -11.8\ cm^{-1}$ was obtained for **3** from the Ising spin-chain model. In accordance with molecular orbital (MO) considerations, much spin density was found to be delocalized not only on the cyclopentadienyl ligand but also the cyano substituents. The magnetic interaction was interpreted as a Heitler–London spin exchange and was analyzed based on how the interaction depends on the singly occupied MOs and the shift of parallel metallocenes relative to each other.

Keywords: cyclic voltammetry · magnetic chains · metallocenes · NMR spectroscopy · stacked molecules

Introduction

Metallocenes, bis(arene) metal compounds, and similar molecules with different π ligands are appealing building blocks for new magnetic materials, because various spin states occur depending on the metal center and the substituent on the ligands. Generally, new bulk magnetic properties result from both ferromagnetic and antiferromagnetic interactions between the building blocks depending on whether like and unlike spin centers are fixed in proximity. The interactions may be realized by linking, for example, metallocenes. Though this approach usually requires tedious synthetic procedures, one can also think of intermolecular magnetic interactions. But so far, these interactions are virtually negligible owing to unfavorable next-neighbor orientations of the metallocenes in the lattice. Herein, we demonstrate that this orientation can be changed to create new properties.

As long as the two π ligands of, for example, a neutral metallocene are essentially parallel, the magnetism corresponds closely to the spin-only value. Intermolecular inter-

[a] Dipl.-Chem. S. Altmannshofer, Dipl.-Phys. R. Miller, Dr. E.-W. Scheidt, Prof. Dr. W. Scherer
Lehrstuhl für Chemische Physik und Materialwissenschaften
Universität Augsburg
86159 Augsburg (Germany)

[b] Dr. E. Herdtweck, Prof. Dr. F. H. Köhler, Dr. R. Mölle
Department Chemie
Technische Universität München
85747 Garching (Germany)
Fax (+49) 89-2891-3762
E-mail: f.h.koehler@lrz.tu-muenchen

[c] Dr. C. Train
Laboratoire de Chimie Inorganique et Matériaux Moléculaires
UMR CNRS 7071, Université Pierre et Marie Curie
4 Place Jussieu, 75252 Paris (France)

Supporting information for this article is available on the WWW under http://www.chemeurj.org/ or from the author.

actions that could be exploited for designing special magnetic behavior are negligible over a large temperature range. This behavior applies to the most-thoroughly studied examples, such as the parent metallocenes,[1] some alkylated congeners,[2] and uranocene,[3] and the same can be safely assumed for paramagnetic bis(arene) metal compounds[4] and mixed-ligand sandwiches,[5] all of which show essentially spin-only magnetism at ambient temperature. Occasionally, orbital magnetism and spin crossover[6] must be considered to properly describe sandwich compounds, but nevertheless, these compounds are magnetically isolated, except for manganocene[7] whose ligands are not parallel and are partly bridging.

Intermolecular magnetic and other interactions depend on the nature and number of close contacts between adjacent species, that is, on the crystal packing. Well-known examples are nitronyl nitroxide radicals that feature overall ferromagnetic or antiferromagnetic behavior.[8] The crystal packing of the parent sandwich compounds is dominated by the shape of the organic ligands and may, therefore, be understood by looking at crystalline benzene. The mutual orientation of neighboring benzene molecules (Figure 1, left) is

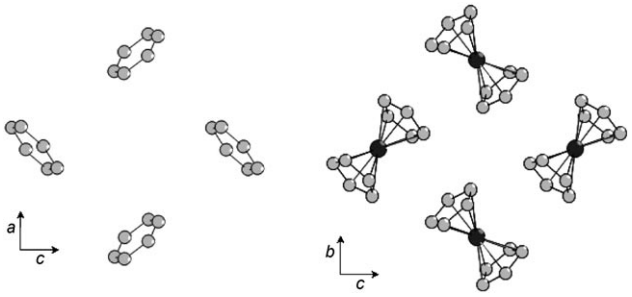

Figure 1. Organization of benzene[9] (left) and metallocene[11d] (right) molecules in the crystal. $[M(C_5H_5)_2]$ M = V, Cr, Fe, Co, Ni.

almost perfectly at right angles,[9] a packing that has been studied for many years.[10] The metallocenes mentioned above pack in much the same way (Figure 1, right) with slight deviations from the perpendicular arrangement depending on the crystal system,[11] and the same is true for other sandwich compounds.[12] Braga and Grepioni[13] showed that the packing principles described for arenes by Kitaigorodsky[10a] are also valid for metallocenes. Considering the magnetic properties of sandwich molecules, it follows that the arrangement at right angles minimizes, if not excludes, magnetic interactions and that π stacking, that is, the face-to-face arrangement of sandwiches, would be desirable to change this behavior. For pure organic radicals, π stacking as illustrated in Figure 2a has been realized, and the experimental and theoretical reports have been reviewed.[14] Sandwich molecules have also been forced into stacks, which was only possible through an electron-transfer reaction with disc-shaped acceptor molecules that slip into the stacks (Figure 2b).[15] Another option would be to assemble pure, magnetically interacting sandwich π stacks (Figure 2c) by introducing substituents with suitable directing properties. We have now realized the latter option by synthesizing cyanometallocenes whose magnetic interactions are tied to the solid state.

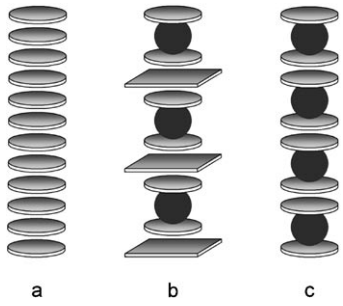

Figure 2. Idealized stacking motives: a) organic π–radical stack, b) sandwich–donor π-acceptor stack, c) sandwich stack.

Another motivation for investigating paramagnetic cyanometallocenes is their potential use as spin-delivering nitrile ligands of diamagnetic and paramagnetic transition-metal ions. Whereas 1,1′-dicyanometallocenes would lead to coordination polymers, the assembly of many unpaired electrons in a discrete species may be envisaged with monocyanometallocenes. Both types of compounds are discussed herein.

Results and Discussion

Syntheses of cyanoferrocenes, cobaltocenes, and nickelocenes: A number of standard reactions are known to substitute arenes with cyano groups, and, correspondingly, 1,1′-dicyanoferrocene has been synthesized from the acid $[Fe(C_5H_4COOH)_2]$.[16] Because this reaction sequence would not be tolerated by the analogous cobaltocenes and nickelocenes without decomposition, we chose an alternative route starting from the $[C_5H_4CN]^-$ ion. Some salts of $[C_5H_4CN]^-$ have been obtained[17] either from dicyclopentadienedicarboxylic acid or $[C_5H_5]^-$ and ClCN, and we recently investigated $K(C_5H_4CN)$ and $Cs(C_5H_4CN)$ in some detail.[18] As the use of the cesium salt has no advantages, $Tl(C_5H_4CN)$[17d] and $K(C_5H_4CN)$ were selected and were treated with iron(II), cobalt(II), and nickel(II) precursor compounds (Scheme 1).

The known 1,1′-dicyanoferrocene[19] (**1**) was needed as a reference compound for the study of paramagnetic analogues 1,1′-dicyanocobaltocene (**2**) and 1,1′-dicyanonickelocene (**3**). In all cases, the reaction of the transition-metal halides with $K(C_5H_4CN)$ gave better yields

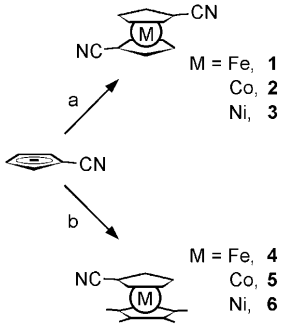

Scheme 1. Syntheses of cyanometallocenes. a) $FeCl_2 \cdot 1.5\,THF$, $CoBr_2$ or $NiBr_2 \cdot 1.5\,THF$; b) $[Fe(C_5Me_5)Cl(tmeda)]$, $[Co(C_5Me_5)(acac)]$, or $[Ni(C_5Me_5)(acac)]$. M = Fe, Co, or Ni.

(49–58%) than with $Tl(C_5H_4CN)$ (31–38%). Unlike the parent metallocenes, the cyano derivatives **1–3** were poorly soluble in hexane, toluene, diethyl ether, and ethanol, whereas the solubility of these derivatives was much better in dichloromethane, nitromethane, *N*-methyl-2-pyrrolidinone (NMP), and dimethyl sulfoxide (DMSO; 30–35 $g\,L^{-1}$). The resulting solutions of **1–3** were orange, dark brown, and green, respectively. The yields of the 1-cyano-1′,2′,3′,4′,5′-pentamethylmetallocenes **4** and **5** were superior (ca. 80%), probably owing to the increased solubility of the components. The synthesis of 1-cyano-1′,2′,3′,4′,5′-pentamethylnickelocene (**6**) was less successful because **6** and decamethylnickelocene were formed in about equal amounts. After repeated chromatographic runs, a sample was obtained whose elemental analysis was in reasonable agreement with those calculated for **6**, but the ^1H NMR spectrum revealed 4% decamethylnickelocene in the sample. The difficulties of isolating **6** are a result of the ease of ligand exchange of $[C_5H_4CN]^-$ (see the NMR spectroscopic studies below).

Table 1. Electrochemical data of cyanoferrocene compounds **1** and **4**, cyanocobaltocenes **2** and **5**, and cyanonickelocenes **3** and **6** in propionitrile.[a]

	Compound					
	1	**4**	**2**	**5**	**3**	**6**
$E_{pc}(0/-1)$	−2.58	[b]	−1.59	−2.36	−1.06	−2.33
$E_{1/2}(0/+1)$	–	0.08	−0.55	−1.25	–	−0.48
$\Delta E_p(0/+1)$	–	0.069	0.068	0.075	–	0.078
I_{pa}/I_{pc}	–	1.05	1.08	1.02	–	1.07
$E_{pa}(0/+1)$	0.80	–	–	–	0.50	–
$E_{pa}(+1/+2)$	[b]	[b]	[b]	[b]	[b]	0.51

[a] Given in volts; the potentials are relative to the couple $[Fe(C_5H_5)_2]/[Fe(C_5H_5)_2]^+$; supporting electrolyte: 0.1 M n-Bu_4NPF_6, scan rate: 200 $mV\,s^{-1}$, temperature: 295 K; E_{pc} or E_{pa}, respectively, are given for the cathodic and anodic peak potentials of irreversible ETs. [b] Not observed.

Redox properties: The new paramagnetic sandwiches **2**, **3**, **5**, and **6** proved to be very reactive, as expected from known congeners. However, the solubility tests seemed to indicate that **2** was not as air-sensitive as the parent cobaltocene. The new compounds were investigated by cyclic voltammetry for quantitative characterization of their stability.

A representative cyclic voltammogram (CV) is given for **2** in Figure 3, whereas other examples are available in the Supporting Information (see Figures SI1–SI4). After comparison with the CV of pure **2**, the main features in Figure 3 were assigned to cobaltocene, the internal standard, and to the electron transfer (ET) processes of **2**, thus resulting in

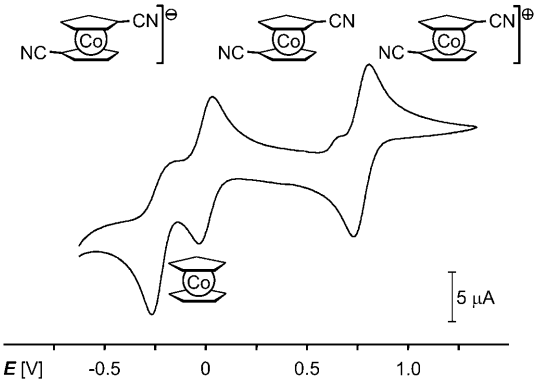

Figure 3. Cyclic voltammogram of a mixture of 1,1′-dicyanocobaltocene (**2**) and cobaltocene in EtCN at 295 K and 200 $mV\,s^{-1}$. The scale is relative to the couple $[CoCp_2]/[CoCp_2]^+$. For the stability ranges of **2**, see text.

the corresponding ions $\mathbf{2}^+$ and $\mathbf{2}^-$. It turns out that **2** is 0.77 V less reducing than the parent cobaltocene, which substantiates its empirically higher stability. Similarly, the reduction of **2** occurs at −0.27 V relative to −1.11 V[20] for cobaltocene. Under the conditions chosen, the reduction of **2** is chemically not reversible and the ET feature of a decomposition product shows up at 0.65 V. However, given the positive potential shift, a tetracyanocobaltocene anion might be isolable. To compare the CV results with those of other compounds, the data have been calculated relative to the ferrocene/ferrocenium couple and summarized in Table 1. Thus, with $E_{1/2}$ values of 0, −1.33, and −0.44 V for $[Fe(C_5H_5)_2]/[Fe(C_5H_5)_2]^+$, $[Co(C_5H_5)_2]/[Co(C_5H_5)_2]^+$, and $[Ni(C_5H_5)_2]/[Ni(C_5H_5)_2]^+$ in propionitrile,[21] respectively, it follows from the comparison with the $E_{1/2}$ values of **4** (0.08 V), **5** (−1.25 V), and **6** (−0.48 V) that the positive potential shift of one CN substituent is roughly compensated by that of five methyl groups. An ET shift of 0.4 V per CN group is calculated from the $E_{1/2}(0/1)$ values of **2** and **5**. The same behavior holds for pairs **1** and **4** and **3** and **6**, although these data are less reliable because the oxidation to 1,1′-dicyanoferrocenium and 1,1′-dicyanonickelocenium ions is not reversible. Qualitatively, the ETs of the nickelocenes correspond to those of the ferrocene compounds. Both the reduction and oxidation processes are irreversible with two cyano groups, whereas the oxidation becomes reversible with one cyano and five methyl groups. Based on the assumption that the donor solvent propionitrile might facilitate the metal–ligand cleavage, nickelocene **3** was also studied in 1,2-difluorobenzene. However, this solvent had almost no effect on the reversibility of the ETs.

Solid-state and solution NMR Studies: It has been outlined previously that the NMR signal shifts of paramagnetic molecules are a measure of the unpaired electron spin density at the nucleus under study.[22] It should, therefore, be possible to investigate for the cyanometallocenes how well the spin is delocalized to the CN donor site and how the spin might be further transmitted to a coordinated metal ion. When passing to the solid state, intermolecular interactions may be studied as well.[23] The effect of unpaired electrons is associated with paramagnetic signal shifts (at the standard temper-

ature 298 K) δ^{para}, which are obtained after subtracting the respective signal shifts of an isostructural diamagnetic molecule from the experimental shifts of the paramagnetic molecule (see the Experimental Section). For this purpose, ferrocene compounds **1** and **4** were studied. The ^{13}C NMR spectra of **1** and **4** showed signals in shift ranges characteristic of (methylated) cyclopentadienyl ligands and cyano substituents. The solid-state signals of the CN groups appeared as two-signal patterns with a 2:1 intensity owing to the ^{14}N second-order quadrupolar effect on the cross-polarized magic-angle spinning (MAS) spectra[24] (see Figures SI5 and SI6 in the Supporting Information). The patterns were simulated[25] by applying a quadrupolar coupling constant of $J = -3.87$ MHz[26] to obtain the signal shifts given in the Experimental Section. The solution- and solid-state ^{13}C NMR signal shifts differed by up to 3.5 ppm, and, therefore, they were used as respective references for the solution- and solid-state spectra of the paramagnetic compounds. Because of the smaller proton shift range, only the signal shifts obtained from the ^{1}H NMR spectroscopic analysis of **1** and **4** in solution served as corresponding references.

The ^{13}C NMR spectrum of 1,1′-dicyanonickelocene (**3**; $S = 1$) in solution (Figure 4) showed a 2:2:1 pattern beyond $\delta = 1300$ ppm for the cyclopentadienyl (Cp) carbon atoms and a signal for the CN group at $\delta = -1100$ ppm. It follows that, as in all nickelocenes, efficient direct delocalization of positive spin occurs to the Cp carbon atoms.[27] The signal splitting for C1–5 is comparatively small because the spin densities in the two singly occupied molecular orbitals (SOMOs) add up to similar values. Yet one MO dominates, which is the basis of the signal assignment (see Figure SI7 in the Supporting Information). Since the spin density at the cyano carbon atom is negative, spin polarization is active in the CN group. It must be concluded that the spin at the cyano nitrogen atom is positive and that further spin transfer from there to some potentially coordinated metal ion would induce negative spin density.

The replacement of one C_5H_4CN ligand for C_5Me_5 in the mixed-ligand nickelocene **6** is associated with a redistribution of the spin density, as can be concluded from the changes in the signal shifts (Table 2). The weighted-average ^{13}C NMR shifts of the Cp carbon atoms $\delta^{para,av}$ is $\delta = 1253$ and 1343 ppm for **6** and **3**, respectively. There is, hence, less spin on the C_5H_4CN ligand of **6**, in particular less at the CN group (cf. $\delta = |-1009|$ versus $|-1195|$ ppm for **6** and **3**, respectively), and **3** would be a better source than **6** for the spin transmission to a metal ion coordinated at the CN donor. The spin density on the C_5H_4CN ligand of **6** decreases at the expense of spin on the C_5Me_5 ligand, which follows from the signal shifts of the methyl carbon atom of **6** and $[Ni(C_5Me_5)_2]$ (cf. $\delta = |-799|$ versus $|-653|$ ppm,[28] respectively).

Table 2. ^{1}H and ^{13}C NMR data of cyanocobaltocenes **2** and **5** and cyanonickelocenes **3** and **6**.[a]

		Compound			
		2	**3**	**5**	**6**
C1	C_7D_8	1239	1517	1208	1464
C1	MAS	798	886	[b]	[b]
C2/5	C_7D_8	−164.6	1250	12.7	1175
C2/5	MAS	−298	844	[b]	[b]
C3/4	C_7D_8	693	1350	588	1226
C3/4	MAS	707	941	[b]	[b]
CN	C_7D_8	−669	−1195	−547	−1009
CN	MAS	−696	−973	[b]	[b]
$C_5(CH_3)_5$	C_7D_8	–	–	525	[c]
$C_5(CH_3)_5$	C_7D_8	–	–	−178.3	−799
H2/5	C_7D_8	7.5	−226.8	−6.6	−166.2
H2/5	MAS	27.4	−176.7	[b]	[b]
H3/4	C_7D_8	−56.2	−249.8	−46.2	−183.4
H3/4	MAS	−60.8	−176.7	[b]	[b]
$C_5(CH_3)_5$	C_7D_8	–	–	41.3	276.4

[a] Paramagnetic signal shifts in ppm at 298 K; signal shifts from saturated solutions in [D$_8$]toluene and isotropic signal shifts from MAS spectra after Herzfeld–Berger analysis. [b] Not measured. [c] Not clear because of an overlap of signals with C1–5.

The solid-state ^{13}C NMR spectrum of **3** proved to be strikingly different (Figure 4). The signal shifts were much smaller than in solution, which was still true after converting the data into δ^{para} values at 298 K (Table 2). In addition, the sequence of the signals of C1–C5 was different from that in solution. The signal shifts from the ^{1}H NMR spectra showed a correspondingly strong decrease on passing from the solution to the solid-state spectra (see Figure SI8 in the Supporting Information and Table 2). The signal intensities of the MAS spectrum suggest that the signals of H2/5 and H3/4 merge. However, there are additional features (not seen in the solution spectrum) that we attribute to the ends of the sandwich chains (see below). It is worth noting that **3** underwent facile ligand exchange with $[NiCp_2]$ to form monocyanonickelocene in solution, as established with ^{1}H NMR spectroscopic analysis (see Figure SI9 in the Supporting Information). This behavior means that the nickel–ligand

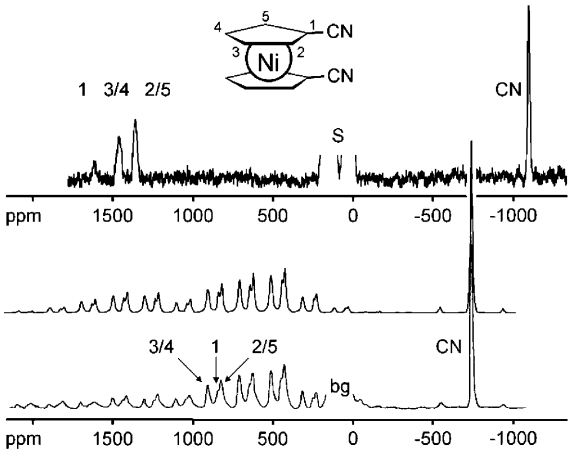

Figure 4. ^{13}C NMR spectra of compound **3**. Top trace: Saturated solution in [D$_8$]toluene at 294 K, S = solvent signals (truncated). Bottom trace: Solid-state spectrum at 335 K, spinning rate: 15 kHz, bg = background signal of the probe head (truncated), nonassigned signals are spinning sidebands. Center trace: Simulated solid-state spectrum.

bond in **3** is rather ionic.[29] Consequently, the less ionic [VCp_2] was used instead of [$NiCp_2$] as an internal temperature standard for recording the NMR spectra.

The analysis of the ^1H and ^{13}C NMR spectra of 1,1′-dicyanocobaltocene (**2**; $S=1/2$;) and 1-cyano-1′,2′,3′,4′,5′-pentamethylcobaltocene (**5**) is straightforward (Figure 5), whereas

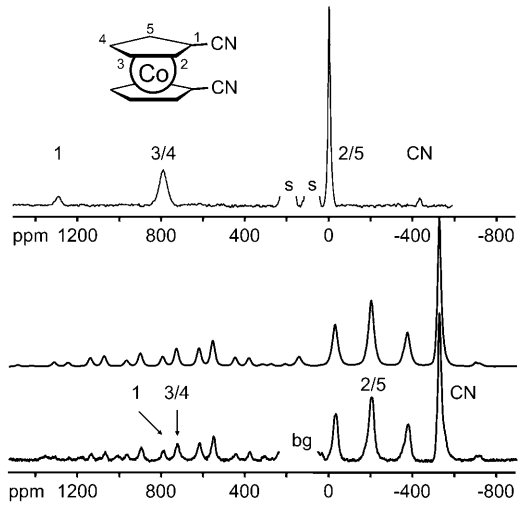

Figure 5. ^{13}C NMR spectra of compound **2**. Top trace: Saturated solution in CH_3CN at 294 K, S = solvent signals (truncated). The signal intensity for CN is low, because the emitter frequency was adjusted close to the signal of C1. Bottom trace: Solid-state spectrum at 323 K, spinning rate: 13 kHz, bg = background signal of the probe head (truncated), non-assigned signals are spinning sidebands. Center trace: Simulated solid-state spectrum.

the comparison of the spectra of **2** and **5** and the differences between the solution and solid-state spectra of **2** are more complex. The same type of MOs as for the nickel analogue **3** are relevant for the assignment of the signals from the ^{13}C NMR spectra (see Figure SI7 in the Supporting Information). Now there is only one SOMO, thus implying that the spin-density sequence is C1 > C3/4 ≫ C2/5. The population of the next higher MO (with the inverse spin-density sequence C2/5 > C3/4 ≫ C1) has been taken into account by studying the temperature dependence of the paramagnetic signal shifts from the ^1H NMR spectra (see Figure SI10 in the Supporting Information). The fact that there is only a minor deviation from the Curie behavior means that the unpaired electron is restricted essentially to the MO with the spin-density sequence C1 > C3/4 ≫ C2/5. Actually, C2/5 receives so little positive spin density that polarization of the electrons in the bonds between C2/5 and C1 and between C2/5 and C3/4 through spin at C1 and C3/4 leads to an overall negative spin density at C2/5. This behavior is reflected in the negative signal shift for C2/5, whereas the signal shifts for C3/4 and C1 are positive, as expected. The ^1H NMR spectra of **2** (see Figure SI11 in the Supporting Information) show signals with positive (H2/5) and negative shifts (H3/4; see Table 2) and confirm the spin distribution in the ligand. In the solid state (unlike in solution), the signal of H3/4 seems to be split. The origin of the splitting is unknown, but one may speculate that this has to do with the ends of the sandwich chains mentioned for the corresponding nickel derivative (cf. the magnetic studies below).

When going from **2** to **5**, a spin redistribution similar to that described for **3** and **6** is expected. Indeed, the dicyano derivative would again be a better spin-releasing nitrile ligand than the monocyano derivative, as can be concluded from the signal shifts of the CN groups of **2** and **5** (cf. $\delta = |-669|$ versus $|-547|$ ppm, respectively). However, the signal shifts for C1–C5 of the C_5H_4CN ligand change more strikingly when passing from **2** to **5** (Table 2). This behavior cannot be a result of different MO populations because the temperature-dependent ^1H NMR shifts of **5** and **2** (see Figure SI12 in the Supporting Information) are very similar. Rather the spin redistribution also affects the Cp moiety.

It is enlightening to describe the differences between the solution and solid-state NMR spectra by the average shifts of the NMR signals $\delta^{para,av}$ of the Cp carbon ring and hydrogen atoms (see Table 3 and the Supporting Information). In the solid state, all the average signal shifts are smaller, which means that the spin density is decreased. This finding in turn points to intermolecular magnetic interactions and some special arrangement of the molecules in the crystal lattice.

Table 3. Mean shifts of the ^1H and ^{13}C NMR signal [ppm] of the Cp ring atoms for **2** and **3** in solution and as powders.

		$\delta^{para,av}$ (C ring)	$\delta^{para,av}$ (H ring)
2	C_7D_8	459	−35
2	MAS	323	−28
3	C_7D_8	1343	−246
3	MAS	891	−177

Crystal structure of 1,1′-dicyanometallocenes: Single crystals of 1,1′-dicyanoferrocene (**1**) big enough for X-ray investigation were grown by cooling a solution of **1** in acetonitrile, whereas numerous attempts to obtain crystals of the cobalt and nickel derivatives **2** and **3** failed. The molecular structure of **1** (Figure 6) is surprising in that the conformation is virtually eclipsed (torsion angle C1···D···D′···C1′: −2.2°). Accordingly, the idealized symmetry is C_{2v} with a D-Fe-D′ angle of 176.9° (D = centroid of the Cp ring) slightly opening the sandwich at the cyanide positions. Note that metallocenes have a low barrier to ring rotation so that in the average solution structure the CN groups would adopt *trans* positions (Scheme 1 and Figure 3). The distances between the iron center and the carbon atoms of the Cp unit in **1** reflect a significant slippage of the Cp ligands, such that the iron atom is shifted toward the CN groups. The reason is that the first antibonding MO of the $[C_5H_4CN]^-$ ligand has a large coefficient not only at C1 but also at C6 and that its energy is much lower than that of the next antibonding MO. Therefore, the first MO mixes more strongly into the relevant bonding MO of **1,** and the iron atom moves toward C1 and C1′ (for details see the Supporting Information).

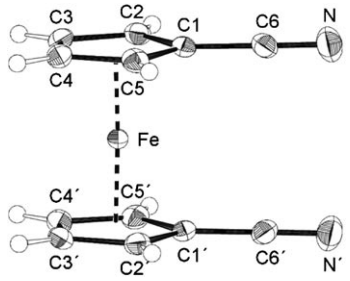

Figure 6. Structure of compound **1** (ORTEP plot) in the solid state. Thermal ellipsoids are drawn at the 50% probability level. The symmetry operation to generate equivalent atom positions is $1-x$, y, $1/2-z$. Selected bond lengths [Å] and angles [°]: Fe–C1 2.038(2), Fe–C2 2.056(2), Fe–C3 2.064(2), Fe–C4 2.061(2), Fe–C5 2.055(2), C1–C6 1.429(2), N–C6 1.150(2); D-C1-C6 179.7, C1-C6-N 179.5(2), C2-C1-C6 125.8(2), C5-C1-C6 125.5(2).

The sandwiches in the crystal are arranged in parallel planes with all the cyano groups pointing in the same direction (Figure 7). This behavior is in striking contrast to the

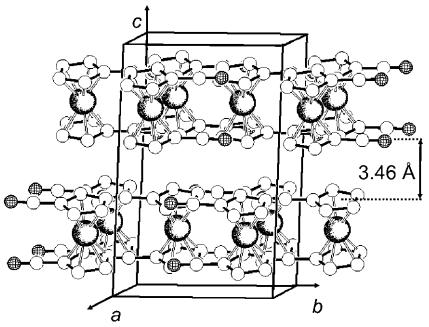

Figure 7. Packing of molecule **1** in the crystal.

usual sandwich arrangement at right angles mentioned in the Introduction. The respective cyano groups of **1** in adjacent planes point in opposite directions. The distance between the Cp rings of adjacent planes is 3.46 Å, which would suggest an intermolecular interaction little less than between the carbon planes of graphite (3.35 Å). However, the sandwiches do not form perfect pillars as represented in Figure 2. Rather the sandwiches are shifted relative to each other, such that, after projection in a common plane, the iron atoms of adjacent sandwiches are separated by 1.06 Å, which would decrease intermolecular interactions. From the crystal structure of **1**, it follows that one way of achieving π-stacked packing of sandwich molecules seems to require a stick-shaped substituent at each ring. With only one cyano substituent per metallocene,[30] the packing corresponds to that of the parent metallocenes (Figure 1).

The crystal structure of the analogous cobalt and nickel derivatives **2** and **3** is expected to correspond to **1** because the structures of metallocenes with the same substitution patterns are usually isotypic, and the series $[MCp_2]$ (except M = Mn) is a well-known example.[11] We have verified this outcome for **1** and **2** by applying X-ray powder methods (see the Supporting Information). Both molecules crystallize in the space group $C2/c$, with the volume of the unit cell of the cobalt derivative being about 2% larger than that of the iron analogue. This corresponds to the increase of the metal–ligand distances in the metallocene series M = Fe, Co, Ni, which depends on the electron count.[31]

Magnetic studies: Since the π stacking of solid 1,1′-dicyanometallocenes was suspected to be responsible for the magnetic interactions evident from the NMR spectroscopic studies, cobalt and nickel derivatives **2** and **3** were subjected to magnetic measurements. The magnetic behavior of 1,1′-dicyanocobaltocene (**2**) is strikingly different from its unsubstituted congener, which we measured for comparison (Figure 8a and b). Upon decreasing the temperature, the $\chi_m T$ value (χ_m = molar magnetic susceptibility) of $[CoCp_2]$ decreases linearly from 0.37 $cm^3 K mol^{-1}$ at 300 K to 0.35 $cm^3 K mol^{-1}$ at 130 K in line with a spin-only value of $S = 1/2$. Below 100 K, $\chi_m T$ decreases somewhat faster and saturates at 0.26 $cm^3 K mol^{-1}$ below 11 K, which is smaller than the ideal spin-only value (0.376 $cm^3 K mol^{-1}$) of an $S = 1/2$ compound. Our measurements confirm those of König

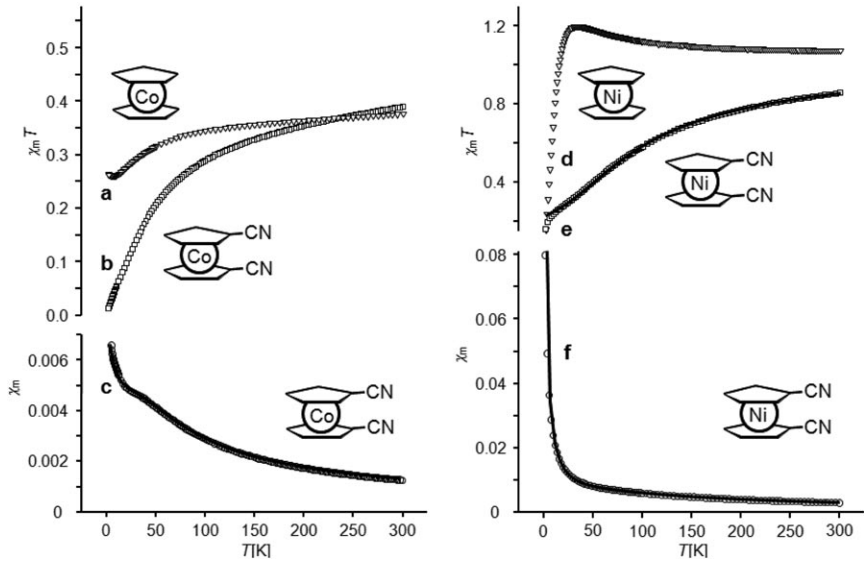

Figure 8. Magnetic behavior of cobaltocene (left) and nickelocene (right) compounds. Temperature dependence of $\chi_m T$ (in $cm^3 K mol^{-1}$) of **2** (trace b) relative to that of $[CoCp_2]$ (trace a). Temperature dependence of χ_m (in $cm^3 mol^{-1}$) of **2** with the theoretical curve (both trace c). Temperature dependence of $\chi_m T$ (in $cm^3 mol^{-1} K$) of **3** with the theoretical curve (both trace e) relative to that of $[NiCp_2]$ (trace d). Temperature dependence of χ_m (in $cm^3 mol^{-1}$) of **3** with the theoretical curve (both trace f).

et al. who ascribed this behavior to ligand-field distortion.[32] By contrast, the $\chi_m T$ value at room temperature for the dicyano derivative **2** ($\chi_m T = 0.39\ cm^3 K mol^{-1}$) is slightly bigger than expected and decreases more and more rapidly until it reaches $\chi_m T = 0.014\ cm^3 K mol^{-1}$ at 2 K.

A qualitatively very similar behavior was observed for the corresponding pair of nickelocenes (Figure 8d and e). In the case of [$NiCp_2$], the product $\chi_m T$ increases from virtually the spin-only value for an $S=1$ compound ($\chi_m T = 1.03\ cm^3 K mol^{-1}$ at 300 K) to $1.19\ cm^3 K mol^{-1}$ at 33 K and then rapidly drops to $0.157\ cm^3 K mol^{-1}$ at 2 K. This behavior confirms previous results that were interpreted to be a result of zero-field splitting, thus causing the steep drop,[1d–f] and competitive, weak intermolecular ferromagnetic and antiferromagnetic interactions.[1f] As expected for intermolecular interactions, the ferromagnetic hump near 30 K disappears when [$NiCp_2$] is diluted in [$MgCp_2$].[33] By contrast, the $\chi_m T$ value of 1,1′-dicyanonickelocene (**3**) at 300 K is only $0.81\ cm^3 K mol^{-1}$ and gradually decreases to $0.159\ cm^3 K mol^{-1}$ at 2 K.

For both 1,1′-dicyanometallocenes **2** and **3**, the comparison of the $\chi_m T$ versus T curves with those observed for the unsubstituted derivatives indicates that an antiferromagnetic interaction is superimposed on the single-ion effects. According to the NMR spectroscopic results, the interaction must be intermolecular. The π-stacked organization of the molecules in the crystal suggested describing the interaction with a one-dimensional model.[34] In the present case, the maximum χ_m value expected at low temperature is partly masked by other effects. Probably the most pronounced perturbation is a result of defects in the lattice, thus creating chain ends that behave as an admixture of paramagnetic monomers.[35] Actually, the ^1H MAS NMR spectra of **2** and **3** (see Figures SI11 and SI8, respectively, in the Supporting Information) show features that are not seen in solution and that may be attributed to such chain ends.

To fit the susceptibility of 1,1′-dicyanometallocenes over the whole temperature range, we assumed that the observed temperature-dependent magnetic susceptibility χ_m is mainly a result of the linear chains, but altogether consists of three terms [Eq. (1)]:

$$\chi_m = \chi_{IC}(1-f) + \chi_{CW} f + \text{TIP} \quad (1)$$

where χ_{IC} is the isotropic-chain susceptibility, χ_{CW} is a Curie–Weiss component that arises from the terminal spins of finite-length chains that are exchange coupled to the respective last-but-one chain member, and TIP is the Van Vleck paramagnetism of the open-shell metal ions. The parameter f represents the fraction of chain ends mentioned above. In the case of **2**, an approach based on $S=1/2$ infinite isotropic Heisenberg chain (Bonner–Fisher susceptibility[36]) is appropriate. There are no analytical solutions for the magnetic susceptibility of the Heisenberg chains, but a useful approximation has been suggested by Estes et al. [Eq. (2a)]:[35b]

$$\chi_{IC} = \frac{N g_{av}^2 \mu_B^2}{k_B T} \frac{0.25 + 0.14995\,x + 0.30094\,x^2}{1 + 1.9862\,x + 0.68854\,x^2 + 6.0626\,x^3} \quad (2a)$$

where $x = |J|/k_B T$, N is the Avogadro number, g_{av} is the mean g factor, μ_B is the Bohr magneton, k_B is the Boltzmann constant, J is the magnetic exchange coupling constant, and T is the absolute temperature. A comparable expression has been proposed in the case of $S=1$ infinite isotropic Heisenberg chains.[37] It is readily adapted for compound **3** [Eq. (2b)] :

$$\chi_{IC} = \frac{N g_{av}^2 \mu_B^2}{k_B T} \frac{2 + 0.0302\,x + 0.8997\,x^2}{3 + 4.5452\,x + 2.7477\,x^2 + 6.9038\,x^3} \quad (2b)$$

The Curie–Weiss-like contribution is given by Equation (3).

$$\chi_{CW} = \frac{N g_{av}^2 \mu_B^2 S(S+1)}{3\,k_B (T-\theta)} \quad (3)$$

where S is the spin quantum number and θ is the Weiss temperature. The experimental data could be well reproduced by using the fitting parameters J, g_{av}, and f, supplemented by θ, and the TIP for **2** (cf. Figure 8, trace c) with the values given in Table 4.

Table 4. Parameters obtained from fitting the magnetic data of **2** and **3**.

	[$Co(CpCN)_2$] (**2**)	[$Ni(CpCN)_2$] (**3**)	
Chain model	Heisenberg	Heisenberg	Ising
J [cm^{-1}]	−28.3	−10.3	−11.8
g	1.94	2.06	2.05
f	0.17	0.21	0.25
θ [K]	−11.4	–	–
TIP [$cm^3 mol^{-1}$]	229×10^{-6}	–	–
chain length	14	12	10

It is gratifying that the parameter of main interest, J, proved to be robust during the fitting. When θ and TIP were neglected, $J = -30.4\ cm^{-1}$ was obtained (instead of $-28.3\ cm^{-1}$), whereas the low-temperature part of the fitting curve deviated somewhat from the experimental points, and $g=1.64$ (instead of 1.94) was unusually small. Actually, the final data fit was supported by the EPR spectrum (see Figure SI17 in the Supporting Information), which reflects the rhombic distortion expected from the low symmetry of the molecule. The g factors of **2** ($g_x = 2.068$, $g_y = 2.012$, $g_z = 1.884$[38]) are well within the range found for four other substituted cobaltocenes,[39] and the average value $g_{av} = 1.98$ is close to $g = 1.94$ obtained from the magnetic data fit.

For the nickel derivative **3** with $S=1$, Heisenberg and Ising chain models are available.[36] These models differ mainly in the susceptibility at and near $T=0$, at which the Heisenberg model leads to a plateau of the χ_m curve, whereas it drops to zero in the Ising model. Inspection of the experimental data (Figure 8) shows that these criteria are masked by the low-temperature divergence of χ_m because of

the effect of the chain ends mentioned above. Therefore, both models were applied and gave similar results (Table 4). The robustness of the fits was ensured by simultaneous fitting of the experimental $\chi_m T$ and χ_m data. It is worth noting that the mean g factor of 2.05–2.06 corresponds to that of $[NiCp_2]$.[1d,f] A Haldane gap has not been considered in the fits because the strong zero-field splitting known for nickelocenes makes its appearance unlikely.[40] The composition of the fitting curves is documented in the Supporting Information (see Figures SI17 and SI18).

The J parameters derived from the fits do not only establish a rather strong antiferromagnetic coupling within solid **2** and **3** but also confirm that its origin is a pure molecular crystal effect. Thus, the same chain model of π-stacked sandwiches applies in both cases. The fraction f of chain ends (Table 4) is equivalent to an average chain length of 10–14 stacked molecules, which is close to the 11 spin centers taken into account for the Heisenberg approximation used herein.

Molecular orbital consideration: For a qualitative understanding of the face-to-face interaction of solid 1,1′-dicyanometallocenes, it is useful to discuss the relevant SOMOs. In the case of nickelocenes, we start from $[NiCp_2]$, which has two degenerate SOMOs. Generally, they split upon symmetry lowering through substitution, in the present case with two cyano ligands in **2** and **3**. Herein, we limit the discussion to **3**. When two molecules are arranged in a stack to form the model dimer **3**···**3**, further orbital splitting yields four SOMOs, that is, two **3**···**3** bonding combinations, MO70 and MO72 shown in Figure 9, and their **3**···**3** antibonding counterparts, MO69 and MO71 not shown. At a given **3**···**3** distance (assumption: 3.46 Å as in **1**), the intermolecular interaction, as reflected by the MO splitting, depends on the shape of the respective MO and on the relative orientation of the components **3**. This behavior is illustrated in the lower part of Figure 9, in which a relative shift of 0 Å means that the Cp–Ni axes are colinear. Upon shifting the lower nickelocene between −9 and 4 Å (perpendicular to the chain direction), the energies of MO70 and MO72 behave differently. The electron density of the ligand in MO70 is concentrated at C2–C5 and just one broad energy minimum is seen. By contrast, the electron density in MO72 is localized at C3/4, C1, and the cyano group, thus giving rise to four energy minima. As expected, the energy curves of antibonding MO69 and MO71 are virtually mirror images of MO70 and MO72, respectively. It follows that if the relative shift of adjacent 1,1′-dicyanonickelocenes is similar to that of **1** (dotted line in Figure 9), they are arranged for close to maximal intermolecular interactions (see broken curve in Figure 9).

The discussion of changes in spin density following from intermolecular interactions must include the sign of the spin density at the respective atoms, which is not obtained from simple extended Hückel calculations. The signs of the spin density follow, however, from the NMR spectra as the signal shifts are a measure of the spin densities.[22] Previously, we

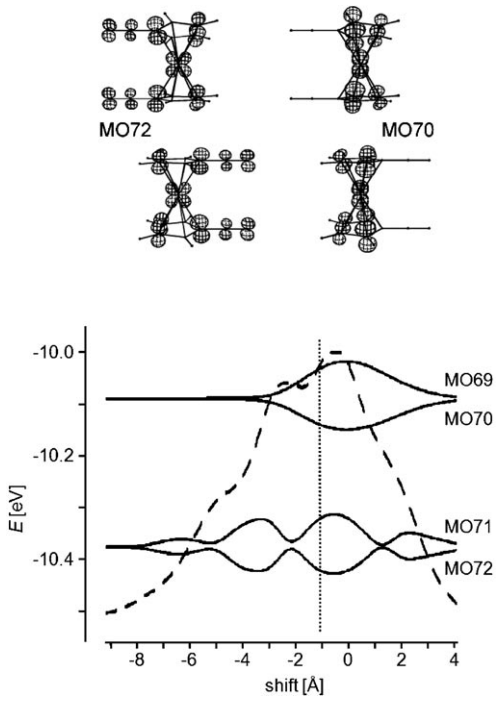

Figure 9. Top: Selected SOMOs of two stacked 1,1′-dicyanonickelocenes **3**···**3**. Bottom: SOMO energy changes of **3**···**3** upon shifting one moiety **3** relative to the other (see text). The broken curve represents the total energy change and the dotted line marks the relative shift of two adjacent stacked metallocenes found for the iron analogue **1**.

have shown that paramagnetic sandwich cations can transmit spin density to neighboring counterions and that spin in a π orbital of one species (tetracyanoethylenide) can be transmitted to the π orbitals of another species (decamethylcobaltocenium ion).[23] A similar situation is met for two adjacent cyanocyclopentadienyl ligands of two cobaltocenes and nickelocenes arranged as **2**···**2** and **3**···**3**, respectively, whose spin distribution is represented in Figure 10. When the sandwiches are shifted as found for the iron analogue **1**, it is obvious that the intermolecular interactions in **2**···**2** should be different from those in **3**···**3**. For the analysis of local spin interactions, it is helpful to recall that according to the Heitler–London spin exchange antiferromagnetic in-

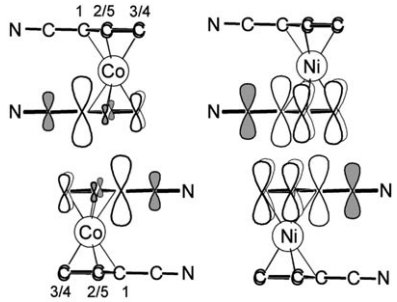

Figure 10. Spin densities at the carbon atoms of the adjacent cyanocyclopentadienyl ligands of two stacked cobaltocenes **2**···**2** and nickelocenes **3**···**3**. The positive and negative spin densities are white and gray, respectively.

teractions are expected when the spin at neighboring sites has the same sign, whereas ferromagnetic interactions should arise from different spin signs.[41] When this fact is applied to **3**···**3** (Figure 10, right), the magnetic measurements and the decrease of all the absolute NMR signal shifts suggest that the antiferromagnetic interactions of positive spin on the adjacent Cp cores C1–C5 prevail. Things are more complicated for the stacked cobalt derivative **2**···**2** because negative and positive spins alternate within the Cp ring. Accordingly, on passing from solution to the solid state, the absolute NMR signal shift of only the C1 atom decreases whereas the shifts for all the other atoms increase (Table 2). Computations at a level that is higher than the extended Hückel approach used herein might clarify the local interactions; however, these calculations are beyond the scope of this report. On the other hand, the NMR spectroscopic data of paramagnetic metallocenes were reproduced by applying DFT methods[42] and were related quantitatively to spin densities.[43]

Conclusion

Cyanocyclopentadienide is a reliable reagent for the synthesis of metallocenes, even if the products are very sensitive. The cyano substituents efficiently modify the reactivity of the metallocenes: nickelocenium and ferrocenium ions become less stable, whereas the metallocene anion and neutral cobaltocene become more stable.

The introduction of stick-shaped cyano substituents also causes a change in the organization of the molecules in the crystal lattice; the arrangement of next-neighbor sandwiches switches from perpendicular to parallel. This behavior entails intermolecular magnetic interactions that are mediated by adjacent spin-containing ligand π orbitals. NMR spectroscopic analysis and magnetic measurements are complementary methods for the study of this sort of crystal packing. The latter method probes the bulk magnetism which in the present case appears as one-dimensional antiferromagnetic interactions within chains of stacked sandwiches. Because of lattice defects, an average chain consists of 10–14 1,1′-dicyanometallocene units. The NMR spectroscopic method probes the local magnetism of an ensemble of equivalent molecules. Hence, the comparison of spectra of dissolved and solid samples constitutes a convenient check for intermolecular magnetic interactions. In addition, the spin transmission to individual nuclei can be followed quantitatively. It turns out that the cyano groups receive much spin density so that paramagnetic cyanometallocenes can be regarded as spin-delivering nitrile ligands.

The spin density on the Cp rings provides a clue to further changes in the crystal packing. If areas of positive and negative spin density exist on a given Cp ligand, as in the case of 1,1′-dicyanocobaltocene, appropriate shifting of the stacked sandwiches would place the negative spin of one sandwich close to the positive spin density of the adjacent sandwich. This scenario favors ferromagnetic interactions.[41] Likewise, assembling stacks of, for example, alternating nickelocenes and vanadocenes through co-crystallization would also lead to ferromagnetic interactions because in the ligand π orbitals of nickelocenes the spin is positive, whereas it is negative for vanadocenes.[27b]

Experimental Section

Procedures and characterization: The syntheses and investigations of the compounds were performed in a purified, dry dinitrogen atmosphere by using Schlenk-type glassware, which had been dried at 140 °C prior to use.

Unless otherwise noted, the solution NMR spectra of the diamagnetic compounds were recorded on a Jeol JNM GX 270 spectrometer, and the solution NMR spectra of the paramagnetic compounds on a Bruker AV 300 spectrometer, which was equipped with MAS probeheads for solid-state spectra, including those of the ferrocene compounds, and solenoid probeheads for solution spectra. Tubes modified as described previously[44] were used for placing the solutions at right angles to the magnetic field. ZrO_2 and Si_3N_4 rotors (4 mm) packed in a glove box were used for the MAS NMR spectroscopic experiments. All NMR signal shifts of the solution spectra were measured relative to solvent signals and calculated relative to trimethylsilane (TMS) by using $\delta(CH_3)=2.49$ ppm and $\delta(CH_3)=39.5$ ppm for [D$_6$]DMSO and $\delta(CH_3)=2.03$ ppm and $\delta(CH_3)=20.4$ ppm for [D$_8$]toluene. All signal shifts from solid-state NMR spectra were measured relative to external adamantane and calculated relative to TMS by using $\delta(CH)=2.0$ ppm and $\delta(CH)=29.5$ ppm. In the case of the dissolved and solid paramagnetic compounds, this procedure gave experimental signal shifts at the measuring temperature δ_T^{exp}, which were calculated relative to the corresponding signals of the analogous ferrocene compounds to give the paramagnetic signal shifts δ_T^{para}. The temperature was determined by adding 3–5 wt % of [Ni(C$_5$H$_5$)$_2$] to the samples and measuring the shift in the ^{1}H NMR signals of Cp$_2$N. The temperature calibration has been reported for solid samples.[43,45] The temperature calibration for samples in solution is $T=-77132/(\delta_T^{para}=-1.04)$ (see the Supporting Information). The cyanonickelocenes were studied by using [V(C$_5$H$_5$)$_2$] as an internal temperature standard.[45] The solid-state NMR spectra were analyzed and simulated by using the programs HBA and Wsolids, respectively.[46] The IR and mass spectra were obtained from Perkin-Elmer 1600 FTIR and Varian MAT 50 spectrometers, respectively.

The magnetic measurements were obtained from Quantum Design MPMS7 ([CoCp$_2$] and **2**) and MPMS5 ([NiCp$_2$] and **3**) SQUID magnetometers. The samples were measured in a helium atmosphere in the range 1.8–300 K and external magnetic fields of 1 and 0.3 T, respectively. The obtained values (Figure 8) were corrected for the diamagnetic moment of the empty sample holder and the core diamagnetism calculated from the Pascal constants ($\chi_{dia}=-142\times10^{-6}$ cm^{3}mol^{-1} for [CoCp$_2$], $\chi_{dia}=-158\times10^{-6}$ cm^{3}mol^{-1} for **2**, $\chi_{dia}=-140\times10^{-6}$ cm^{3}mol^{-1} for [NiCp$_2$], and $\chi_{dia}=-156\times10^{-6}$ cm^{3}mol^{-1} for **3**).

The cyclic voltammograms (CVs) were recorded with a computer-controlled potentiostat 173/276 from Princeton Applied Research, a homemade cell with cooling jacket, a Ag/AgCl reference electrode, a combined Pt counter and working electrode, and a device for drying the solution within the cell immediately before running the CV. The drying agent was Al_2O_3 (Super I N, no. 04580; ICN, Essen, Germany). The compounds were dissolved in a 0.1 M nBu$_4$NPF$_6$ in propionitrile with concentrations close to 1.3 mmol L^{-1} in all cases. The potentials were measured in separate runs after the addition of ferrocene relative to the potential of [Fe(C$_5$H$_5$)$_2$]/[Fe(C$_5$H$_5$)$_2$]$^+$, except for **2** and **6**, which were measured relative to [Co(C$_5$H$_5$)$_2$]/[Co(C$_5$H$_5$)$_2$]$^+$ and calculated relative to [Fe(C$_5$H$_5$)$_2$]/[Fe(C$_5$H$_5$)$_2$]$^+$ with $E_{1/2}=-1.32$ V for [Co(C$_5$H$_5$)$_2$] in propionitrile at 295 K. All the potentials were reproducible within a range of 15 mV or better, and mean values are reported. The elemental analyses were carried out by the microanalytical laboratory of the Faculty of Chemistry,

Garching. The extended Hückel calculations were carried out with the program package CACAO, version 4.0.[47]

Materials: All reagents were commercially obtained except for the following, which were synthesized according to literature procedures: $Li(C_5Me_5)$,[48] $K(C_5H_4CN)$,[18] $Tl(C_5H_4CN)$,[17d] $FeCl_2{\cdot}1.5\,THF$,[49] $NiBr_2{\cdot}1.5\,THF$,[50] $[FeCl(C_5Me_5)(tmeda)]$ (tmeda = *N*,*N*-tetramethylethylenediamine),[51] $[Co(C_5Me_5)(acac)]$ (acac = acetylacetonate),[52] and $[Ni(C_5Me_5)(acac)]$.[53] The solvents were dried by standard methods and freed from dioxygen by distilling under a stream of dinitrogen.

1,1′-Dicyanoferrocene (1): $Tl(C_5H_4CN)$ (3.00 g, 10.2 mmol) was added to a stirred suspension of $FeCl_2{\cdot}1.5\,THF$ (1.49 g, 6.4 mmol) in THF (100 mL). When the gray–brown reaction mixture was stirred and heated to reflux for 24 h, the liquid phase became yellow after a few minutes and finally orange. After the mixture had been cooled to room temperature, the liquid was filtered and the residue was washed with portions of THF (20 mL) until the liquid was colorless. The combined solutions of THF were evaporated under vacuum. The brown remainder was extracted with toluene (3×50 mL), two thirds of the solvent was evaporated, and the solution was kept at −20 °C until a powder had separated. After filtration and removal of the residual solvent from the solid at 10^{-2} bar, **1** was obtained as a light orange microcrystalline compound (294 mg). When the remaining solution was reduced to a volume of 15 mL and cooled, a further aliquot of **1** was obtained (165 mg). The overall yield was 38% relative to $Tl(C_5H_4CN)$. Compound **1** was obtained in 58% yield after starting from $K(C_5H_4CN)$.[19c] M.p. 160–162 °C; ^{1}H NMR (270 MHz, [D$_6$]DMSO, 305 K): δ = 5.03 (pseudo t, ^{2+4}J(H,H) = 3.8 Hz, 4H; H3/4 or H2/5), 4.69 (pseudo t, ^{2+4}J(H,H) = 3.8 Hz, 4H; H2/5 or H3/4) ppm; ^{13}C NMR (67.8 MHz, [D$_6$]DMSO, 305 K): δ = 118.9 (CN), 74.3 and 73.8 (C3/4 and C2/5), 54.5 (C1) ppm; CP-MAS ^{13}C NMR (75.5 MHz, ν_{rot} = 15 kHz, 335 K): δ = 117.1 (ω_Q = 208 Hz, CN), 74.8 (C2–C5), 57.0 (C1) ppm; IR (KBr): $\tilde{\nu}$ = 2224 cm^{-1} (C≡N); MS (CI, 150 eV): *m/z* (%): 236 (100) [M^+], 209 (35) [M^+−CNH], 149 (4) [M^+−C_5N_4CN], the experimental and theoretical isotope patterns of [M]$^+$ were in agreement; elemental analysis (%) calcd for $C_{12}H_8N_2Fe$ (236.05): C 61.06, H 3.42, N 11.87; found: C 61.07, H 3.31,N 11.74

1,1′-Dicyanocobaltocene (2): **Procedure A**: Anhydrous $CoBr_2$ (1.50 g, 6.9 mmol) was suspended in THF (50 mL) and a solution of $K(C_5H_4CN)$ (1.42 g, 11.0 mmol) in THF (50 mL) was added under stirring. At room temperature, the reaction mixture became green–brown after a few minutes and black after heating to reflux for 5 h. The reaction mixture was cooled to room temperature and filtered. The remaining solid was washed with portions of THF (20 mL) until the liquid was colorless, the solvent was removed from the combined solutions under vacuum, and the solid was extracted with toluene (100 mL) in a Soxhlet apparatus. When the solution thus obtained was concentrated under reduced pressure to 50 mL and cooled to −20 °C, a black solid precipitated slowly. After filtration and drying under vacuum, **2** was obtained as a microcrystalline powder (393 mg). Further concentration of the remaining toluene solution to 10 mL and cooling to −20 °C gave another aliquot of **2** (250 mg). The overall yield of **2** was 49% relative to $K(C_5H_4CN)$.

Procedure B: The synthesis described above for 1,1′-dicyanoferrocene was carried out with $CoBr_2$ (1.90 g, 8.7 mmol) suspended in THF (200 mL) and $Tl(C_5H_4CN)$ (4.09 g, 13.9 mmol). The reaction mixture changed from light blue to green–brown and finally to dark brown. The two-step yield of **2** was 420 and 115 mg or 32% relative to $Tl(C_5H_4CN)$.

M.p. 189–190 °C (decomp); ^{1}H NMR (300 MHz, [D$_8$]toluene, 301.6 K) δ^{exp} [half width, Hz] = 12.3 [230] (4H; H2/5), −50.7 [450] (4H; H3/4) ppm; CP-MAS ^{1}H NMR (300 MHz, ν_{rot} = 14.9 kHz, 335.0 K): δ^{exp} [half width, Hz] = 29.2 [2160] (4H, H2/5), −49.2 [2210] (4H; H3/4) ppm; ^{13}C NMR (75.5 MHz, CH_3CN, 293.7 K) δ^{exp} [half width, Hz] = 1311 [1830] (2C; C1), 777 [2650], (4C; C3/4), −93.2 [820] (4C; C2/5), −560 [2210] (2C; CN) ppm; CP-MAS ^{13}C NMR (75.5 MHz, ν_{rot} = 13 kHz, 323.3 K): δ^{exp} [half width, Hz] = 792 [1760] (2C; C1), 726 [1770] (4C; C3/4), −200 [2300] (4C; C2/5), −523 [1450] (2C; CN) ppm; IR (KBr): $\tilde{\nu}$ = 2210 cm^{-1} (C≡N); MS (CI, 150 eV): *m/z* (%): 239 (100) [M^+], 212 (22) [M^+−CNH], 149 (13) [M^+−C_5N_4CN], the experimental and theoretical isotope patterns of [M^+] were in agreement; elemental analysis (%) calcd for $C_{12}H_8N_2Co$ (239.14): C 60.27, H 3.37, N 11.71; found: C 60.34, H 3.30, N 11.65

1,1′-Dicyanonickelocene (3): **Procedure A**: Procedure A described above for 1,1′-dicyanocobaltocene was carried out with $NiBr_2{\cdot}1.5\,THF$ (1.45 g, 4.5 mmol) suspended in THF (80 mL) and $K(C_5H_4CN)$ (0.92 g, 7.12 mmol) in THF (80 mL). The reaction mixture changed from orange to olive and finally to dark green. The two-step yield of **3** was 274 and 169 mg or 52% relative to $K(C_5H_4CN)$.

Procedure B: Procedure B described above for 1,1′-dicyanocobaltocene was carried out with $NiBr_2{\cdot}1.5\,THF$ (1.44 g, 4.4 mmol) suspended in THF (200 mL) and $Tl(C_5H_4CN)$ (2.08 g, 7.06 mmol). The reaction mixture changed in a similar manner to that of procedure A. The two-step yield of **3** was 164 and 94 mg or 31% relative to $Tl(C_5H_4CN)$.

M.p. 170–173 °C (decomp); ^{1}H NMR (300 MHz, [D$_8$]toluene, 301.6 K) δ^{exp} [half width, Hz] = −219.2 [690] (4H; H2/5), −242.0 [660] (4H; H3/4) ppm; CP-MAS ^{1}H NMR (300 MHz, ν_{rot} = 14.9 kHz, 335.0 K): δ^{exp} [half width, Hz] = −152 [4230] (8H; H2–H5) ppm; ^{13}C NMR (75.5 MHz, CH_3CN, 293.7 K) δ^{exp} [half width, Hz] = 1594 [1250] (2C; C1), 1444 [2980] (4C; C3/4), 1342 [2140] (4C; C2/5), −1093 [1140] (2C; CN) ppm; CP-MAS ^{13}C NMR (75.5 MHz, ν_{rot} = 15 kHz, 335.0 K): δ^{exp} [half width, Hz] = 845 [2230] (2C; C1), 911 [2000] (4C; C3/4), 825 [2000] (4C; C2/5), −748 [1240] (2C; CN) ppm; IR (KBr): $\tilde{\nu}$ = 2217 cm^{-1} (C≡N); MS (CI, 150 eV): *m/z* (%): 238 (100) [M^+], 211 (91) [M^+−CNH], 149 (52) [M^+−C_5N_4CN], the experimental and theoretical isotope patterns of [M^+] were in agreement; elemental analysis (%) calcd for $C_{12}H_8N_2Ni$ (238.90): C 60.33, H 3.38, N 11.73; found: C 60.59, H 3.46, N 11.77.

1-Cyano-1′,2′,3′,4′,5′-pentamethylferrocene (4): A solution of $K(C_5H_4CN)$ (0.71 g, 5.5 mmol) in THF (20 mL) was added dropwise to a solution of $[Fe(C_5Me_5)Cl(tmeda)]$ (1.89 g, 5.5 mmol) in toluene (40 mL). Where the drops hit the surface, the yellow-green mixture turned orange immediately and a microcrystalline solid formed. After the addition of the reagent, the orange reaction mixture was stirred at ambient temperature for 1 h, then the solvent was removed at 10^{-2} bar, and the solid remainder was extracted with hexane (100 mL). The extraction was completed by washing the solid with portions of hexane (15 mL) until the liquid was colorless. The solvent was evaporated from the combined solutions under vacuum until a volume of 30 mL. When this solution was allowed to stand at −20 °C, an orange microcrystalline solid formed. Filtration and drying at 10^{-2} bar gave **4** (945 mg). After reducing the remaining solution to a volume of 10 mL and cooling, another aliquot of **4** (305 mg) was obtained. The overall yield of **4** was 81% relative to $[Fe(C_5Me_5)Cl(tmeda)]$. M.p. 76–78 °C; ^{1}H NMR (270 MHz, [D$_8$]toluene, 305 K): δ = 3.65 (pseudo t, ^{2+4}J(H,H) = 3.8 Hz, 2H; H3/4 or H2/5), 3.42 (pseudo t, ^{2+4}J(H,H) = 3.8 Hz, 2H; H2/5 or H3/4), 1.62 (s, 15H; CH_3) ppm; ^{13}C NMR (67.8 MHz, [D$_8$]toluene, 305 K): δ = 119.4 (CN), 81.9 (CCH_3) 74.2 and 74.1 (C3/4 and C2/5), 55.2 (C1), 10.2 (CCH_3) ppm; CP-MAS ^{13}C NMR (75.5 MHz, ν_{rot} = 15 kHz, 335 K): δ = 117.6 (ω_Q = 195 Hz, CN) 80.5 (CCH_3), 74.5 and 72.9 (C2/5 and C3/4), 51.9 (C1), 10.2 (CCH_3) ppm; IR (KBr): $\tilde{\nu}$ = 2210 cm^{-1} (C≡N); MS (CI, 150 eV): *m/z* (%): 281 (100) [M^+], 266 (5) [M^+−CH_3], 191 (11) [M^+−C_5N_4CN], the experimental and theoretical isotope patterns of [M^+] were in agreement; elemental analysis (%) calcd for $C_{16}H_{19}NFe$ (281.18): C 68.35, H 6.81,N 4.98; found: C 68.00, H 6.77, N 4.95.

1-Cyano-1′,2′,3′,4′,5′-pentamethylcobaltocene (5): The procedure described for **4** was carried out with $[Co(C_5Me_5)(acac)]$ (2.91 g, 9.9 mmol) and $K(C_5H_4CN)$ (1.41 g, 10.9 mmol) in toluene (100 and 50 mL, respectively) and by heating to reflux for 10 h. The reaction mixture changed from yellow-red to red-brown, and the two-step yield of **5** was 1.35 and 0.89 g or 79% relative to $[Co(C_5Me_5)(acac)]$. M.p. 70–72 °C; ^{1}H NMR (300 MHz, [D$_8$]toluene, 344.6 K) δ^{exp} [half width, Hz] = 37.3 [90] (15H; CH_3), −2.3 [100] (2H; H2/5), −36.3 [140] (2H; H3/4) ppm; ^{13}C NMR (75.5 MHz, [D$_8$]toluene, 327.2 K) δ^{exp} [half width, Hz] = 1155 (noisy signal) (1C; C1), 609.3 [790] (2C; C3/4), 560.2 [820] (5C; CCH_3), 85.7 [340] (d, ^1J(C,H) = 153 ± 14 Hz, 2C; C2/5), −152.2 [370] (q, ^1J(C,H) = 111 ± 14 Hz, 5C; CCH_3), −378.3 [430] (1C; CN) ppm; IR (KBr): $\tilde{\nu}$ = 2194 cm^{-1} (C≡N); MS (CI, 150 eV): *m/z* (%): 284 (100) [M^+], 194 (13) [M^+−C_5H_4CN], 133 (13) [$C_5Me_5^+$−2H], the experimental and theoretical isotope patterns of [M^+] were in agreement; elemental analysis (%)

calcd for $C_{16}H_{19}NCo$ (284.27): C 67.60, H 6.74, N 4.93; found: C 67.55, H 7.03, N 4.45.

1-Cyano-1′,2′,3′,4′,5′-pentamethylnickelocene (6): The procedure described for **5** was carried out with $[Ni(C_5Me_5)(acac)]$ (2.18 g, 7.4 mmol) and $K(C_5H_4CN)$ (1.06 g, 8.2 mmol). The reaction mixture changed from dark red to green-brown. After workup, a 1:1 mixture of $[Ni(C_5Me_5)_2]$ and **6** was obtained according to ^{1}H NMR spectroscopic analysis. A sample of the solid mixture (0.5 g) was dissolved in hexane (2 mL) and subjected to column chromatography on Al_2O_3 with Et_2O as the eluent. Two colored bands developed, the first was dark green and contained $[Ni(C_5Me_5)_2]$ ($\delta^{exp}_{295.7}(^1H) = 243.6$ ppm),[28] the second band was lighter green. The solvent was removed from the latter band, and the remainder was purified by column chromatography again under the same conditions. Collecting the second band and removal of the solvent gave a green microcrystalline powder (120 mg), which comprised 97% **6** and 4% $[Ni(C_5Me_5)_2]$ as shown by ^{1}H NMR spectroscopy. The calculated yield of **6** was 6% relative to $[Ni(C_5Me_5)(acac)]$. M.p. 37–40 °C; ^{1}H NMR (300 MHz, [D$_8$]toluene, 331.2 K) δ^{exp} [half width, Hz] = 250.3 [640] (15 H; CH_3) −146.0 [590] (2 H; H2/5), −161.7 [570] (2 H; H3/4) ppm; ^{13}C NMR (75.5 MHz, [D$_8$]toluene, 293.8 K) δ^{exp} [half width, Hz] = −800.3 [370] (5 C; CCH_3) −904.3 [430] (1 C; CN) ppm; further partly overlapping signals at $\delta = 1540$, 1246, and 1318 ppm could not be assigned to the four expected five-membered carbon ring atoms because of the low signal-to-noise ratio and large signal widths; IR (KBr): $\tilde{\nu} = 2214$ cm^{-1} (C≡N); MS (CI, 150 eV): *m/z* (%) for **6**: 283 (100) [M^+], 193 (2) [$M^+ - C_5H_4CN$], 133 (13) [$C_5Me_5^+ - 2H$], the experimental and theoretical isotope patterns of [M^+] were in agreement; elemental analysis (%) calcd for 96% $C_{16}H_{19}NNi$ (284.02) + 4% $[Ni(C_5Me_5)_2]$ (329.15): C 67.91, H 6.86, N 4.70; found: C 68.71, H 6.93, N 4.75.

Single-crystal and powder X-ray studies: Crystal data and details of the structure determination are presented in Table 5. Suitable single crystals for the X-ray diffraction study were grown from acetonitrile. A clear orange needle was stored under perfluorinated ether, transferred in a Lindemann capillary, fixed, and sealed. Preliminary examination and data collection were carried out on an area detecting system (NONIUS, MACH3, κ-CCD) at the window of a rotating anode (NONIUS, FR591) and graphite-monochromated $Mo_{K\alpha}$ radiation ($\lambda = 0.71073$ Å). Data collection was performed at 223 K (Oxford Cryosystems) within a Θ range of $3.44 < \Theta < 26.32°$. Six data sets were measured in rotation scan modus with $\Delta\phi/\Delta\Omega = 2.0°$. A total number of 9295 intensities were integrated. Raw data were corrected for Lorentz, polarization, and, arising from the scaling procedure, for latent decay and absorption effects. After merging ($R_{int} = 0.034$) a sum of 955 (all data) and 931 ($I_o > 2\sigma(I_o)$), respectively, remained and all the data were used. The structure was solved by a combination of direct methods and difference Fourier syntheses. All non-hydrogen atoms were refined with anisotropic displacement parameters. All hydrogen atoms could be located in the difference Fourier maps and were allowed to refine freely. Full-matrix least-squares refinements with 85 parameters were carried out by minimizing $\Sigma w(F_o^2 - F_c^2)^2$ with the SHELXL-97 weighting scheme and stopped at shift/err < 0.001. The final residual electron-density maps showed no remarkable features. Neutral atom scattering factors for all atoms and anomalous dispersion corrections for the non-hydrogen atoms were taken from the *International Tables for Crystallography*.[54]

CCDC-662374 (**1**) contains the supplementary crystallographic data for this paper. These data can be obtained free of charge from The Cambridge Crystallographic Data Centre via www.ccdc.cam.ac.uk/data_request/cif.

A Guinier diffractometer equipped with an imaging plate detector (HUBER G670) and $Mo_{K\alpha 1}$ radiation ($\lambda = 0.7093$ Å) was used for collecting the powder X-ray data of **2** (see the Supporting Information).

Table 5. Summary of the crystal data, details of data collection, and structure refinement for **1**.

formula	$C_{12}H_8FeN_2$
M_r	236.05
crystal shape	orange needle
crystal dimensions [mm]	0.15 × 0.15 × 0.68
crystal system	monoclinic
space group	*C*2/*c* (no. 15)
a [Å]	8.9356(2)
b [Å]	8.2267(2)
c [Å]	13.2914(3)
β [°]	107.7662(11)
V [Å^3]	930.46(4)
Z	4
T [K]	223
μ [mm^{-1}]	1.579
ρ_{calcd} [g cm^{-3}]	1.685
data collected	9295
independent data ($I_o > 2\sigma(I_o)$/all data/R_{int})	931/955/0.034
data/restraints/parameters	955/0/85
*R*1 ($I > 2\sigma(I_o)$/all data)	0.0229/0.0236
*wR*2 ($I > 2\sigma(I_o)$/all data)	0.0692/0.0697
GOF	1.111
$\Delta\rho_{max/min}$ [e Å^{-3}]	0.78/−0.29

Acknowledgements

We thank Prof. A. Lerf for preliminary X-ray powder studies. This study was generously supported by the Bayerisch–Französisches Hochschulzentrum (R. Mölle) and by NanoCat (R. Miller), an International Graduate Program within the Elitenetzwerk Bayern.

[1] a) E. König, V. P. Desai, B. Kannelakopulos, E. Dornberger, *J. Organomet. Chem.* **1980**, *187*, 61–71; b) E. König, V. P. Desai, B. Kannelakopulos, E. Dornberger, *J. Chem. Phys.* **1983**, *78*, 6299–6306; c) E. König, R. Schnakig, S. Kremer, B. Kannelakopulos, R. Klenze, *Chem. Phys.* **1978**, *27*, 331–344; d) R. Prins, J. D. W. van Voorst, C. J. Schinkel, *Chem. Phys. Lett.* **1967**, *1*, 54–55; e) A. V. Zvarykina, Yu. S. Karimov, E. V. Leonova, R. B. Lyubovskii, *Sov. Phys. Solid State* **1970**, *12*, 385–387; f) P. Baltzer, A. Furrer, J. Hulliger, A. Stebler, *Inorg. Chem.* **1988**, *27*, 1543–1548.

[2] a) J. L. Robbins, N. M. Edelstein, S. R. Cooper, J. C. Smart, *J. Am. Chem. Soc.* **1979**, *101*,3853–3857; b) E. König, V. P. Desai, B. Kannelakopulos, F. H. Köhler, *Chem. Phys.* **1980**, *54*, 109–113; c) J. L. Robbins, N. Edelstein, B. Spencer, J. C. Smart, *J. Am. Chem. Soc.* **1982**, *104*, 1882–1893;

[3] a) D. Karraker, *Inorg. Chem.* **1973**, *12*, 1105–1108; b) H. D. Amberger, R. D. Fischer, B. Kanellakopulos, *Theor. Chim. Acta* **1975**, *37*, 105–127; c) N. Edelstein, A. Streitwieser, Jr., D. G. Morrell, R. Walker, *Inorg. Chem.* **1976**, *15*, 1397–1398.

[4] a) E. O. Fischer, U. Piesbergen, *Z. Naturforsch. B* **1956**, *11*, 758–759; b) E. O. Fischer, G. Joos, W. Meer, *Z. Naturforsch. B* **1958**, *13*, 456–457; c) E. O. Fischer, F. Röhrscheid, *Z. Naturforsch. B* **1962**, *17*, 483; d) E. O. Fischer, H. H. Lindner, *J. Organomet. Chem.* **1964**, *2*, 222–229.

[5] a) E. O. Fischer, H. P. Kögler, *Z. Naturforsch. B* **1958**, *13*, 197–198; b) R. B. King, F. G. A. Stone, *J. Am. Chem. Soc.* **1976**, *98*, 1083–1088; c) D. Astruc, J.-R. Hamon, G. Althoff, E. Román, P. Batail, P. Michaud, J.-P. Mariot, F. Varret, D. Cozak, *J. Am. Chem. Soc.* **1979**, *101*, 5445–5447.

[6] a) F. H. Köhler, B. Schlesinger, Inorg. Chem. 1992, *31*, 2853–2859, and references therein; b) H. Sitzmann, M. Schaer, E. Dormann, M. Kelemen, *Z. Anorg. Allg. Chem.* **1997**, *623*, 1850–1852; c) H. Sitzmann, M. Schaer, E. Dormann, M. Kelemen, *Z. Anorg. Allg. Chem.* **1997**, *623*, 1609–1613; d) E. D. Brady, J. S. Overby, M. B. Meredith, A. B. Mussman, M. A. Cohn, T. P. Hanusa, G. T. Yee, M. Pink, *J. Am. Chem. Soc.* **2002**, *124*, 9554–9566.

[7] a) W. Bünder, E. Weiss, *Z. Naturforsch. B* **1978**, *33*, 1235–1237; b) E. König, V. P. Desai, B. Kannelakopulos, R. Klenze, *Chem. Phys.* **1980**, *54*, 109–113.

[8] M. Deumal, J. Cirujeda, J. Veciana, J. J. Novoa, *Chem. Eur. J.* **1999**, *5*, 1631–1642.
[9] a) E. G. Cox, D. W. J. Cruickshank, J. A. S. Smith, *Proc. R. Soc. London Ser. A* **1958**, *247*, 1–21; b) G. E. Bacon, N. A. Curry, S. A. Wilson, *Proc. R. Soc. London, Ser. A* **1964**, *279*, 98–110.
[10] a) A. I. Kitaigorodsky, *Molecular Crystals and Molecules*, Academic Press, New York, **1973**, pp. 170–178; b) J. W. Schroer, P. A. Monson, *J. Chem. Phys.* **2000**, *112*, 8950–8957, and references therein.
[11] a) W. Bünder, E. Weiss, *J. Organomet. Chem.* **1975**, *92*, 65–68; b) P. Sailer, J. P. Dunitz, *Acta. Cryst., Sect. B* **1980**, *36*, 2255–2260; c) R. D. Rogers, J. L. Atwood, D. Foust, M. D. Rausch, *J. Cryst. Mol. Struct.* **1981**, *11*, 183–188; d) K. R. Flower, P. B. Hitchcock, *J. Organomet. Chem.* **1996**, *507*, 275–277.
[12] a) A. Avdeef, K. N. Raymond, K. O. Hodgson, A. Zalkin, *Inorg. Chem.* **1976**, *15*, 1083–1088; b) E. O. Fischer, H. P. Fritz, J. Manchot, E. Priebe, R. Schneider, *Chem. Ber.* **1963**, *96*, 1418–1423; c) G. Engbertson, R. E. Rundle, *J. Am. Chem. Soc.* **1963**, *85*, 481–482.
[13] D. Braga, F. Grepioni, *Organometallics*, **1992**, *11*, 711–718.
[14] a) K. Awaga, M. Kinoshita in *Molecular Magnetism* (Eds: K. Itoh, M. Kinoshita), Kodasha, Tokyo, Gordon and Breach Science Publishers, Amsterdam, **2000**, Chapter 4.2; b) T. Kawakami, K. Yamaguchi, D. Yamaki, Y. Yoshioka in *Molecular Magnetism* (Eds: K. Itoh, M. Kinoshita), Kodasha, Tokyo, Gordon and Breach Science Publishers, Amsterdam, **2000**, Chapter 2.1; c) N. Tyutuylkov, F. Dietz in *Magnetic Properties of Organic Materials* (Ed.: P. M. Lahti), Marcel Dekker, New York, **1999**, Chapter 18; d) K. Yoshizawa in *Magnetic Properties of Organic Materials* (Ed.: P. M. Lahti), Marcel Dekker, New York, **1999**, Chapter 19; e) K. Yamaguchi, T. Kawakami, A. Oda, Y Yoshida in *Magnetic Properties of Organic Materials* (Ed.: P. M. Lahti), Marcel Dekker, New York, **1999**, Chapter 20; f) B. D. Koivisto, R. G. Hicks, *Coord. Chem. Rev.* **2005**, *449*, 2612–2630.
[15] a) V. Gama, M. T. Duarte in *Magnetism: Molecules to Materials, Vol. 5* (Eds.: J. S. Miller, M. Drillon), Wiley-VCH, Weinheim, **2005**, Chapter 1; b) G. T. Yee, J. S. Miller in *Magnetism: Molecules to Materials, Vol. 5* (Eds.: J. S. Miller, M. Drillon), Wiley-VCH, Weinheim, **2005**, Chapter 7.
[16] A. N. Nesmejanow, E. G. Perewalowa, L. P. Jurjewa, *Chem. Ber.* **1960**, *93*, 2729–2734.
[17] a) D. Peters, *J. Chem. Soc. Dalton Trans.* **1960**, 1832–1837; b) O. W. Webster, *J. Am. Chem. Soc.* **1966**, *88*, 3046–3050; c) W. Neukam, W. Grimme, *Tetrahedron Lett.* **1978**, *19*, 2201–2205; d) M. Arthurs, J. C. Bickerton, M. Krikley, J. Palin, C. Piper, *J. Organomet. Chem.* **1992**, *429*, 245–256; e) K. Banert, F. Köhler, B. Meier, *Tetrahedron Lett.* **2003**, *44*, 3781–3783.
[18] E. Herdtweck, F. H. Köhler, R. Mölle, *Eur. J. Inorg. Chem.* **2005**, 952–958.
[19] a) A. N. Nesmeyanov, O. A. Reutov, *Dokl. Akad. Nauk BSSR* **1958**, *120*, 503–506; b) A. N. Nesmeyanov, E. G. Perewalowa, L. P. Jurjewa, *Chem. Ber.* **1960**, *93*, 2729–2734; c) R. E. Christopher, L. M. Venanzi, *Inorg. Chim. Acta* **1973**, *7*, 219–225.
[20] a) W. L. Geiger, Jr., W. L. Bowden, N. El Murr, *Inorg. Chem.* **1979**, *18*, 2358–2361; b) A. J. Bard, E. Garcia, S. Kukharenko, V. Strelets, *Inorg. Chem.* **1993**, *32*, 3528–3531.
[21] H. Atzkern, P. Bergerat, M. Fritz, J. Hiermeier, P. Hudeczek, O. Kahn, B. Kanellakopulos, F. H. Köhler, M. Ruhs, *Chem. Ber.* **1994**, *127*, 277–287.
[22] F. H. Köhler in *Magnetism: Molecules to Materials, Vol. 1* (Eds.: J. S. Miller, M. Drillon), Wiley-VCH, Weinheim, **2001,** Chapter 12.
[23] H. Heise, F. H. Köhler, M. Herker, W. Hiller, *J. Am. Chem. Soc.* **2002**, *124*, 10823–108332.
[24] R. K. Harris, A. C. Olivieri, *Progr. NMR Spectrosc.* **1992**, *24*, 435–456.
[25] WSolids NMR Simulation Package (1.17.22), K. Eichele, R. E. Wasylishen, Dalhousie University, **1999**.
[26] A. Naito, S. Ganapathy, C. A. McDowell, *J. Chem. Phys.* **1981**,*74*, 5393–5397.
[27] a) H. Hilbig, F. H. Köhler, *New J. Chem.* **2001**, *25*, 1152–1162; b) H. Heise, F. H. Köhler, X. Xie, *J. Magn. Reson.* **2001**, *150*, 198–206; c) I. Gattinger, M. A. Herker, W. Hiller, F. H. Köhler, *Inorg. Chem.* **1999**, *38*, 2359–2368; d) J. Blümel, P. Hofmann, F. H. Köhler, *Magn. Reson. Chem.* **1993**, *31*, 2–6.
[28] X. Xie, F. H. Köhler, unpublished results.
[29] M. E. Switzer, M. F. Rettig, *J. Chem. Soc. Chem. Commun.* **1972**, *503*, 687–688.
[30] W. Bell, G. Ferguson, C. Glidewell, *Acta Crystallogr. Sect. A* **1996**, *52*, 1928–1930.
[31] A. Haaland, *Acc. Chem. Res.* **1979**, *12*, 415–422.
[32] E. König, R. Schnakig, S. Kremer, B. Kannelakopulos, R. Klenze, *Chem. Phys.* **1978**, *27*, 331–344.
[33] N. Oswald, Dissertation, Eidgenössische Technische Hochschule, Zürich, **1977**, p. 260.
[34] R. Georges, J. J Borrás-Almenar, E. Coronado, J. Curély, M. Drillon in *Magnetism: Molecules to Materials, Vol. 1* (Eds.: J. S. Miller, M. Drillon), Wiley-VCH, Weinheim, **2001,** Chapter 1.
[35] a) A. P. Ginsberg, *Inorg. Chim. Acta Rev.* **1971**, *5*, 45–68; b) W. E. Estes, D. P. Gavel, W. E. Hatfield, D. J. Godsjon, *Inorg. Chem*, **1978**, *17*, 1415–1421; c) A. Meyer, A. Gleizes, J.-J. Girerd, M. Verdaguer, O. Kahn, *Inorg. Chem.* **1982**, *21,* 1729–1739.
[36] J. C. Bonner, M. E. Fisher, *Phys. Rev.* **1964**, *135*, A640–A658.
[37] D. Beltrán, E. Escrivá, M. Drillon, *J. Chem. Soc. Faraday Trans. 2* **1982**, *78*, 1773–1779.
[38] H.-A. Krug von Nidda, unpublished results.
[39] J. H. Ammeter, *J. Magn. Reson.* **1978**, *30*, 299–325.
[40] a) M. Yamashita, T. Ishii, H. Matsuzaka, *Coord. Chem. Rev.* **2000**, *198*, 347–366; b) J.-P. Renard, L.-P. Regnault, M. Verdaguer in *Magnetism: Molecules to Materials, Vol. 1* (Eds.: J. S. Miller, M. Drillon), Wiley-VCH, Weinheim, **2001,** Chapter 2.
[41] a) H. M. McConnell, *J. Chem. Phys.* **1963**, *39*, 1910; b) J. J. Novoa, M. Deumal, *Struct. Bonding (Berlin)* **2001**, *100*, 33–60.
[42] P. Hrobárik, R. Reviakine, A. V. Arbuznikov, O. L. Malkina, V. G. Malkin, F. H. Köhler, M. Kaupp, *J. Chem. Phys.* **2007**, *126*, 024107/1–024107/19.
[43] H. Heise, F. H. Köhler, X. Xie, *J. Magn. Reson.* **2001**, *150*, 198–206.
[44] a) K. D. Behringer, J. Blümel, *Magn. Reson. Chem.* **1995**, *33*, 729–733; b) F. H. Köhler, B. Metz, W. Strauß, *Inorg. Chem.* **1995**, *34*, 4402–4413.
[45] F. H. Köhler, X. Xie, *Magn. Reson. Chem.* **1997**, *35*, 487–492.
[46] K. Eichele, R. E. Wasylishen, HBA 1.2 and Wsolids, Dalhousie University, Canada, **2001** and **1998**.
[47] C. Mealli, D. M. Prosperio, *Chem. Educ.* **1990**, *67*, 399–402.
[48] F. X. Kohl, P. Jutzi, *J. Organomet. Chem.* **1983**, *243*, 119–121.
[49] C. Le Vanda, K. Bechgaard, D. O. Cowan, U. T. Mueller-Westerhoff, P. Eilbracht, G. A. Candela, R. L. Collins, *J. Am. Chem. Soc.* **1976**, *98*, 3181–3187.
[50] L. G. L. Ward, *Inorg. Synth.* **1972**, *13*, 154–164.
[51] a) K. Jonas, P. Klusmann, R. Goddard, Z. Naturforsch. B **1995**, *50*, 394–404; b) .M. Heigl, PhD thesis, Technische Universität München, München, **2002**.
[52] M. E. Smith, R. A. Andersen, *J. Am. Chem. Soc.* **1996**, *118*, 11119–11128.
[53] E. E. Bunel, L. Valle, J. Manriquez, *Organometallics* **1985**, *4*, 1680–1682.
[54] a) Data Collection Software for NONIUS κ-CCD devices, Delft, The Netherlands, **1997**; b) Z. Otwinowski, W. Minor, *Methods Mol. Med. Methods Enzymology* **1997**, *276*, 307–326; c) *International Tables for Crystallography* (Eds: Th. Hahn, A. J. C. Wilson), Kluwer Academic Publisher, Dordrecht, Boston, London, **1992**; d) L. J. Farrugia, WinGX, *J. Appl. Crystallogr.* **1999**, *32*, 837–838; e) A. L. Spek, PLATON, *A Multipurpose Crystallographic Tool*, Utrecht University, Utrecht, The Netherlands, **2007**; f) A. Altomare, G. Cascarano, C. Giacovazzo, A. Guagliardi, M. C. Burla, G. Polidori, M. Camalli, SIR92, *J. Appl. Crystallogr.* **1994**, *27*, 435–436; g) G. M. Sheldrick, SHELXL-97, University of Göttingen, Göttingen, Germany, **1998**.

Received: September 28, 2007
Revised: April 29, 2008
Published online: July 21, 2008

